ARTICLE IN PRESS

Available online at www.sciencedirect.com

ScienceDirect

ELSEVIER

International Journal of Impact Engineering ▮ (▮▮▮▮) ▮▮▮–▮▮▮

INTERNATIONAL JOURNAL OF IMPACT ENGINEERING

www.elsevier.com/locate/ijimpeng

Experimental and numerical study on the flight and penetration properties of explosively-formed projectile

Jun Wu[a,b,*], Jingbo Liu[a], Yixin Du[a]

[a]*Department of Civil Engineering, Tsinghua University, Beijing 100084, China*
[b]*Luoyang Hydraulic Engineering Technical Research Institute, Luoyang, Henan 471023, China*

Received 3 January 2006; received in revised form 7 April 2006; accepted 10 June 2006

Abstract

The whole process of formation, flying and penetration of explosively-formed projectile (EFP) is simulated by a 3D coupled hydrocode of Ls_dyna. The caliber of the shaped charge is 60 mm and EFP is a kind of overturned shaped charge. The Arbitrary Lagrangian–Eulerian (ALE) method is adopted to consider the fluid–solid coupling problem. The velocity attenuation equation is fitted to forecast the flight distance of EFP. The penetration property of EFP to the armor plate is studied by similarity theory and numerical simulation. For validating the equation, a test is designed to study the residual velocity after penetrating a 25 mm thick steel plate from a distance of 48 m. Therefore, some important solutions are obtained from the comparison of the simulation and experiment. The solutions are optimized charge structure of EFP, the ideal shape of projectile, the attenuation rule of flight process and the penetration property after 48 m flight. The numerical solution fits the experimental data well and the study results provide important reference to the design of EFP in engineering.

Keywords: Explosively-formed projectile (EFP); Penetration; Charge structure; Explosive mechanics

1. Introduction

Explosively-formed projectile (EFP) is a kind of new shaped charge structure which has higher penetration ability and larger explosive distance. The design and theoretical analysis of EFP is a hot problem in the field of weapon engineering [1–3]. Abundant research results indicate that the penetration ability of EFP lies on the shape of projectile, flight property, penetration velocity and others [4–6].

The formation process of EFP is a high pressure and high temperature process. The actions of the charge and its cover are complex because of a lot of influence factors. There are two methods to analyze the formation process of EFP, which are pseudo-stationary uncompressed ideal fluid model and numerical simulation method [7,8]. The formation process of EFP can be analyzed well by the above two methods. But only few papers talked about the flight property and the penetration ability systematically.

*Corresponding author. Department of Civil Engineering, Tsinghua University, Beijing 100084, China. Tel.: +86 10 62772988; fax: +86 10 62771132.

E-mail address: junwu@tsinghua.edu.cn (J. Wu).

0734-743X/$ - see front matter © 2006 Elsevier Ltd. All rights reserved.
doi:10.1016/j.ijimpeng.2006.06.007

In this paper, a series of tests are designed to study the whole process of formation, flying and penetration of EFP. According to the tests, the numerical simulation is carried out using three-dimensional (3D) dynamic finite element program of Ls_dyna. Furthermore, some important solutions are obtained from the comparison of the simulation solution and experimental data, such as the optimized charge structure of EFP, the ideal shape of the projectile, the attenuation rule of the flight process and the penetration property of EFP after 48 m flight distances (800 times of the charge caliber). The numerical solution fits the experimental data well and the study results provide important reference for the engineers to the design of EFP.

2. The parameters and numerical model of the shaped charge

2.1. The influence factors of EFP formation

2.1.1. Charge cover

The charge cover is the most important component for the design of EFP. The material and geometric shape determined the property of the charge cover. Generally, the geometric shape of charge cover can be designed as hemi-spherical, hyperboloid, cone, ballistic disk and other shapes.

After the structure shape of the charge cover is decided, the diameter of the charge cover becomes another critical factor. Larger charge cover has a better penetration effect. But, it costs much more than a small one. The basic aim is to get the smallest structure according to the detailed technical demand.

The thickness of charge cover is another important design variable. Generally, the thickness of cover takes 1–4% of the diameter of shaped charge. Especially, some of the charge cover even has a thickness up to 8% of the diameter of charge. The selection of charge thickness lies on geometric structure, material property, manufacture method and EFP property we wanted. To variable-thickness charge cover, the bad result will occur if the thickness changes suddenly. Therefore, the shape of the cover should be smoothed. Generally, a thin cover has a better effect than a thick cover and it can be accelerated to a high velocity easily.

The material of cover is important to EFP, too. The material must have a property of high melting point, high density, closed crystal structure, good stretch property and no toxicity. The cover always takes the familiar metal material, which is cheap and can be molded easily.

2.1.2. The charge cover's vertex angle

To the cone charge cover, the velocity of EFP becomes higher with the vertex angle decreased, but the effect of the formation gets worse. On the contrary, the velocity of EFP becomes lower with the vertex angle increased and the formation effect gets better.

2.1.3. The length of the charge

The charge alone is enough for the device to have enough explosive energy to melt the charge cover. The charge head height is the distance between the top of shaped charge and the detonating fuse, which must be sufficient to ensure detonation wave becomes plane wave when the explosive wave arrives at the charge cover approximately. The wave arrives at the cover will be a kind of spherical wave if the height is too small. Then, the pressure on the cover is not uniform. The rarefaction wave action in the device will reduce the explosive effect, too. Generally, the velocity of EFP, energy and the penetration depth increase with the increase of the height. But the increase of the penetration depth becomes not evident when the height increases to a certain extent. The penetration depth does not increase after the height over one and a half times of the charge diameter. Therefore, the charge length takes 1.0–1.5 times of the charge diameter. The height of charge head and the length should take the minimum value to reduce the length and the weight of the projectile.

2.1.4. Dynamite loading

There are two main methods used to load dynamite broadly, which are melt-cast and pressed load methods. The density and the grain of the dynamite must be uniform no matter what method we used. There should be no space between the dynamite and the charge cover. Otherwise, there will be some unsymmetrical factors to decrease the ability of EFP.

2.1.5. Ignition method

The ignition method influences formation property of EFP essentially. Different ignition methods will produce different EFP even if the other situations are the same, such as the charge and the charge cover structure. The multi-point ignition method can not only enhance the velocity of the projectile but also increase the ratio of the length to the diameter. Thus, the shape of the projectile empennage will be more perfect. The material of the shaped cover will be damaged and EFP will be broken during the formation process because of the interaction between explosive waves. Therefore, we cannot get the ideal projectile. The radius of multi-point ignition can influence the effect of EFP, too. Generally, the velocity of projectile and the ratio between length and diameter increase when the ignition radius increased.

2.2. The basic dimensions and the parameters of EFP

This paper considers the above conditions synthetically. The computational model and the charge structure are shown in Fig. 1. The basic dimension and the computational parameters of EFP structure are shown as following:

(1) The shape of the charge cover combines arc and cone shapes.
(2) *Basic dimensions*: The length of the charge H is 66 mm, the diameter of the charge D is 60 mm, the diameter of the charge cover h is 56 mm, and the vertex angle of the cone is 140°.
(3) *Material model*: The material of the charge cover is copper and we can take Johnson–Cook material model and Gruneisen equation of state (EOS) in the finite element simulation. The charge is 8710 dynamite and its density ρ is 1845 kg/m^3. We take the High-Explosive-Burn material model and Jones–Wilkins–Lee (JWL) EOS for the dynamite in the numerical simulation. The air elements take the Null material model and Gruneisen EOS. The target plate takes the material of 45# steel and we will take the Plastic-Kinematic model to simulate it in the program. The main parameters of the charge cover and the dynamite are shown in Table 1 [9,10].
(4) *Element model*: The couple of fluid and solid elements is considered in the finite element model. The charge cover is meshed with Lagrange algorithm in the program, the dynamite is meshed with Eulerian algorithm and the air elements between them take the ALE technique.
(5) *Contact type*: In the simulation, sliding contact is used between the charge cover and the dynamite, which is a kind of surface-by-surface contact type.
(6) *Output control*: The termination time of the process is 400 μs and the dynamite element will be deleted after 30 μs. The output interval of the result is 10 μs.
(7) *Ignition method*: The dynamite will be initiated at the center point of the back of the charge and one-point initiation method will be adopted because of the diameter of shaped charge is small.

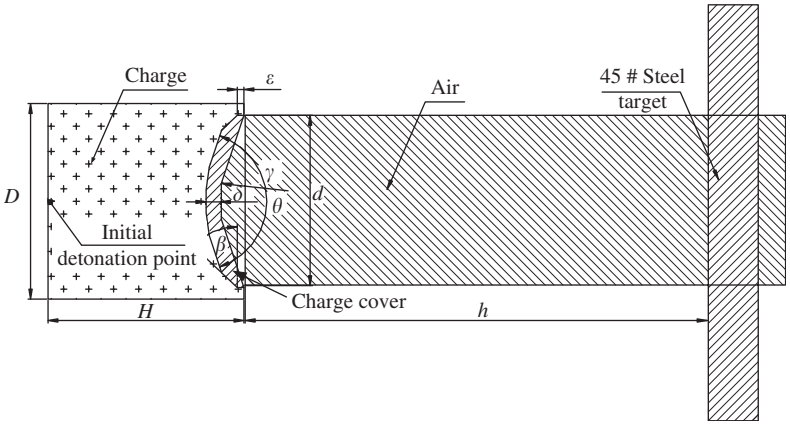

Fig. 1. The computational model of the charge structure.

Table 1
Material property and EOS input data in Dyna

Material	Dyna material types, material property input data and EOS input data (unit = cm, g, μs)								
8701	*MAT_HIGH_EXPLOSIVE_BURN								
	RO	D	PCJ						
	1.680	0.880	0.370						
	*EOS_JWL								
	A	B	R1	R2	OMEG	E0	VO		
	8.524	0.1802	4.550	1.300	0.380	0.085	1.000		
Air	*MAT_NULL								
	RO	PC	MU						
	1.29E−3	0.000	0.000						
	*EOS_LINEAR_POLYNOMIAL								
	C0	C1	C2	C3	C4	C5	C6	E0	V0
	−1.00E6	0.000	0.000	0.000	0.400	0.400	0.000	2.50E−6	1.000
Copper	*MAT_JOHNSON_COOK								
	RO	G	A	B	N	C	M	TM	TR
	8.930	0.464	1.20E−3	0.002	0.150	0.040	0.550	1360.0	293.0
	EPSO	CP	PC	SPALL	IT	D1–D5			
	1.00E−6	3.80E−6	−9.000	3.000	0.000	0.000			
	*EOS_GRUNEISEN								
	C	S1	S2	S3	GAMA	A	E0	V0	
	0.394	1.490	0.000	0.000	1.990	0.000	0.000	0.000	
45# Steel	*MAT_PLASTIC_KINEMATIC								
	RO	E	PR	SIGY	ETAN	BETA	FS		
	7.830	2.070	0.300	0.005	2.07E−4	1.000	0.400		

(8) *Flight distance*: The projectile will fly 48 m before it arrives at the target, which is 800 times of the charge caliber.
(9) *Target plate*: The target plate takes the material of 45# steel and the thickness of the plate is 25 mm. The material of 45# steel is used in China usually and its property is shown in Table 1.

3. The simulation for velocity attenuation law of EFP in air

It will take a lot of time and resource to simulate the entire process of the projectile when it flies a distance of 48 m. It is comparatively operable to simulate just a passage of flying process. Hence, we aim to simulate a flight distance of 0.5 m of EFP to investigate its velocity attenuation law and examine the correctness of the numerical simulation and the feasibility of empirical formula based on experimental data. At last, we try to estimate the velocity at which the shaped charge flies a long distance. The following figure shows the simulated results of the formation process of 60 mm charge caliber EFP. The color of figure indicates the contours of effective stress for 60 mm EFP at different time instants of the formation process from Ls_dyna program.

In light of Fig. 2, when the interaction of shaped charge cover and detonation is finished after 30 μs, the top of the shaped charge flies off before that of the bottom. From this, it can be inferred that the axial velocity of top infinitesimal element is apparently faster than that of the bottom side, forming a turning backward mode. Because the infinitesimal element velocity of the edge is faster than near elements, EFP will produce an extended empennage. The head of the shaped charge can be formed at 110 μs. The central part is elongated and the bottom extends at 200 μs. Therefore, the bacilliform EFP with extended bottom will be shaped. The head of such EFP has good quality of compactness and symmetry while the bottom can take balance during flying. Furthermore, the crush velocity is comparatively slow and axial extension is minor, so the EFP remains good integrality.

Fig. 3 shows a cavum effect when 60 mm EFP flying in air. Fig. 4 shows its attenuation velocity curve based on the simulation.

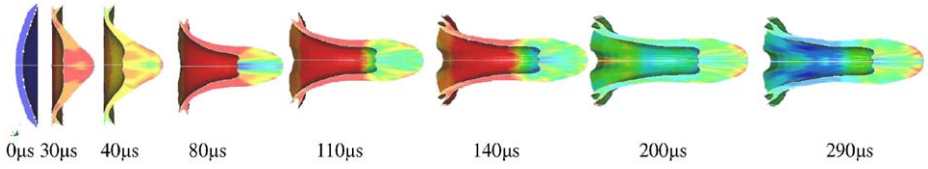

Fig. 2. The formation process of 60 mm charge caliber EFP in the air.

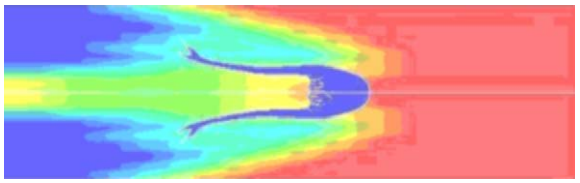

Fig. 3. Cavum effect.

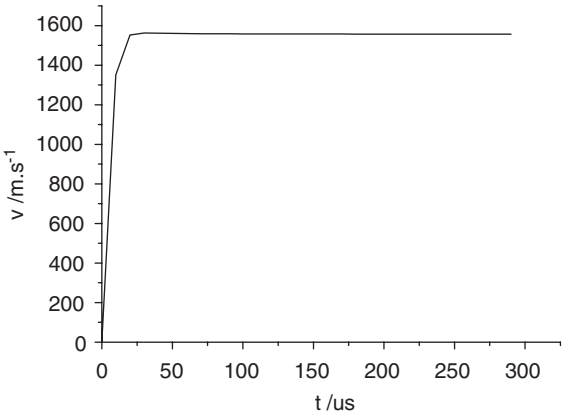

Fig. 4. Velocity curve for initial phase of flight.

Fig. 4 shows that when the velocity of the shaped charge increases to 1563 m/s, there is a stable period of flying. The attenuation curve indicates that the velocity attenuation process can be divided into two phases. The first is velocity attenuation phase, that is, the period of 30–110 μs during which it is in the initial stage of formation with the head and bottom not completely formed, the section is large and in change state, air resistance is strong, so in this period the velocity attenuates fast. Specifically, the velocity decreases from 1563 to 1558 m/s rapidly. During the period of 110–200 μs, the central part is in a state of elongation and the bottom is in a state of extension. In this period, the head has taken shape, section remains the same while the bottom is still extending so the velocity attenuates slowly. The second is stable flying phase, that is, the period of 200–290 μs during which the shaped charge has completely been formed and flies in a stable way. Consequently, during this period the shaped charge receives invariable air resistance and the velocity decreases in such a stable way that it is almost a straight line. The velocity decreases slowly from 1557 to 1556 m/s. In light of the above analysis, the shape of the head and bottom exerts great influence on its velocity attenuation. The velocity attenuation curve is enlarged in Fig. 5 to be seen clearly.

According to the above analysis, an integrated curve shown in Fig. 6 and the empirical velocity equation can be worked out when flying a distance of 0.5 m.

$$
\begin{aligned}
&V_1(t) = 51t \quad (t<30),\\
&V_2(t) = 1569.83 - 0.324t + 0.00363t^2 - (2.155E-5)t^3 + 6.585(E-8)t^4 - (8.23E-11)t^5 \ (30\leqslant t\leqslant 200),\\
&V_3(t) = 1558.26 - 0.0058t \ (t>200).
\end{aligned} \tag{1}
$$

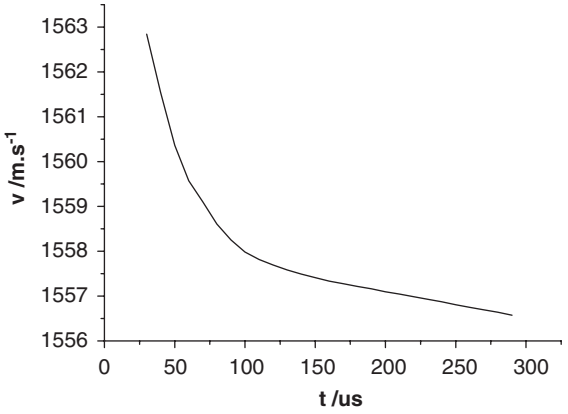

Fig. 5. The velocity attenuation curve of 60 mm EFP.

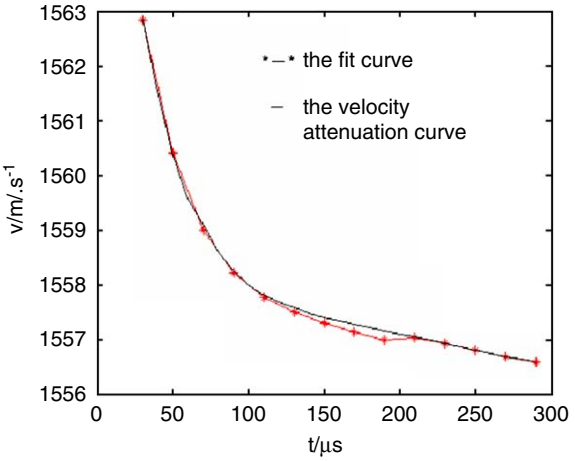

Fig. 6. The fit curve for the velocity attenuation.

During the period of 0–30 μs, the velocity of EFP increases rapidly from 0 to 1553 m/s and the velocity changes as a straight line. The process of flying a distance of 0.5 m can be simply shown in Fig. 7. The following is a formula indicating the flying distance of the shaped charge.

$$S = S_1 + S_2 + S_3 = \int_0^{t_1} V_1(t)d_t + \int_{t_1}^{t_2} V_2(t)d_t + \int_{t_2}^{t} V_3(t)d_t. \tag{2}$$

When S is 0.5 m, we can substitute from formula (2) that $t = 336$ μs, then we can substitute it into Eq. (1) and obtain $V = V_3(336) = 1556.3$ m/s. As EFP likes a column, the following equations can be worked out according to the velocity attenuation equation:

$$\left.\begin{array}{l} V_{\mathrm{R}} = V_0 e^{-aR} \\ a = \frac{C_R \rho S}{m} \\ S = \pi(d/2)^2 \end{array}\right\}, \tag{3}$$

where V_{R} is the velocity when EFP reaches the target (m/s), V_0 is the initial velocity, R is the flight distance when flying in air, a is velocity attenuation coefficient, C_{R} is windward resistance coefficient which is 1.17 for such column shaped charge, ρ is air density which is 1.29 kg/m^3, S is windward area when flying in upright direction (m^2), d is diameter of the EFP (m), and m is its mass (kg).

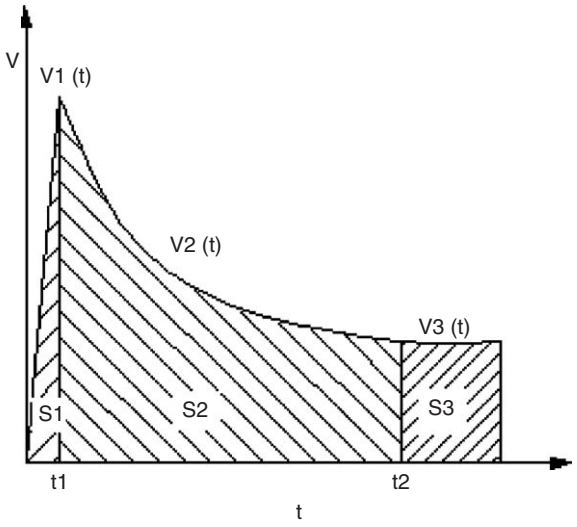

Fig. 7. The velocity attenuation process of EFP.

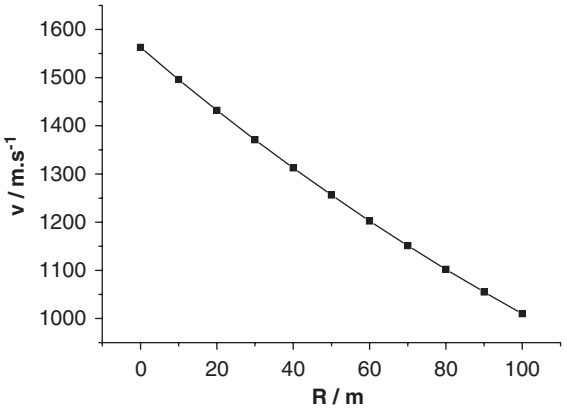

Fig. 8. The velocity attenuation curve of 48 m flight.

Table 2
The shape and velocity parameters of EFP

EFP	V_0 (m/s)	m (kg)	d (mm)	L (mm)	L (d)	$V_{0.5}$ (m/s)	$V_{f-0.5}$ (m/s)	V_{48} (m/s)
60 mm	1563	0.0719	16.7	47.6	2.85	1556.3	1559.9	1267

The parameters of V_0 is 1563 m/s, m is 0.0719 kg and d is 0.0167 m from the numerical simulation of 60 mm EFP. From Eq. (3), we can work out that V_R is 1559.9 m/s. The error is minor which indicates that the above simulation method is appropriate. It is also feasible to predict the velocity when it flies a longer distance with the previous equation. Fig. 8 shows the attenuation rule after 48 m flight.

From the above analysis, the shape and velocity parameters of EFP can be obtained, which are shown in Table 2, where L is the length of the projectile, $V_{0.5}$ is the simulation result of the velocity after 0.5 m flight, $V_{f-0.5}$ is the velocity after 0.5 m flight predicted by Eq. (3) and V_{48} is the predicted velocity of the projectile after 48 m flight.

4. The numerical simulation of the penetration performance of EFP

4.1. The penetration process after 0.5 m flight of EFP

The penetration happens after a long distance flight. Therefore, it is very difficult to simulate the whole process of the ignition, flight and penetration for the projectile. This paper simulates the penetration process of the projectile after 0.5 m flight using a kind of simulated EFP. The penetration performance is studied throughout the whole process simulation and the experiment of the simulated EFP. The feasibility of simulating the penetration process by simulated EFP is discussed, too. The simulated EFP is a scale model of the real EFP by similarity theory. The simulated EFP has the same shape structure as EFP and they have the same initial velocity before penetrating. The parameters for the simulated EFP and real EFP are shown in Tables 3 and 4. The shape of the projectile is shown in Fig. 9.

A 3D solid finite element model is set up to simulate the whole process of the formation of 60 mm EFP, especially 0.5 m flight and the penetration process to the steel target by Ls_dyna. ALE technique is used in the simulation to deal with the coupling problem of the fluid and the solid. On other hand, the penetration process of the simulated EFP and the formatted projectile is simulated using Lagrange grid. The difference of the two kinds of projectile is obtained by the comparison of the simulation result. The penetration model to the steel target is shown in Fig. 9. The penetration process after 0.5 m flight is shown in Fig. 10. The comparison of the penetration process to the steel target between the simulated EFP and real EFP is shown in Fig. 11.

From Fig. 11, we can see that the penetration of the simulated EFP and the real EFP are very similar. Both can be divided into three phases. The first phase is pit-formation around the head of the projectile. The head of

Table 3
The parameters for EFP

Type	Initial velocity V_1 (m/s)	Diameter d (mm)	Length L (mm)	Length/diameter	Mass M (kg)
60 mm	1556	16.7	47.6	2.85	0.072

Table 4
The parameters for the simulated EFP

Mass m (kg)	Margin thickness ε (mm)	Cavum length (L_1) mm	Curvature radius (R_1) mm	Curvature radius (R_2) mm
0.067	3.572	23	39.286	5.952

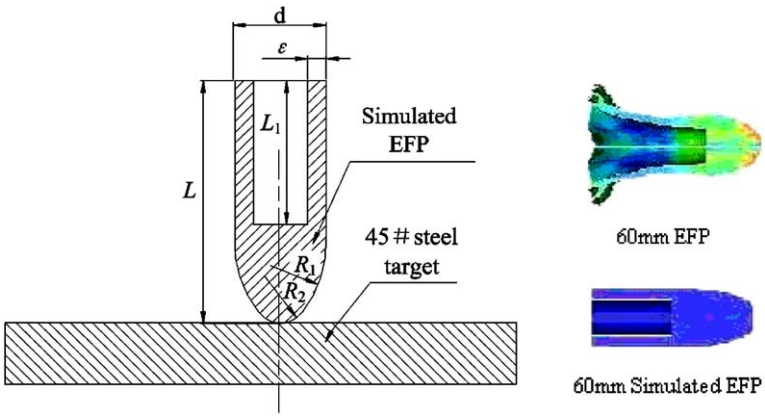

Fig. 9. The penetration model to the steel target.

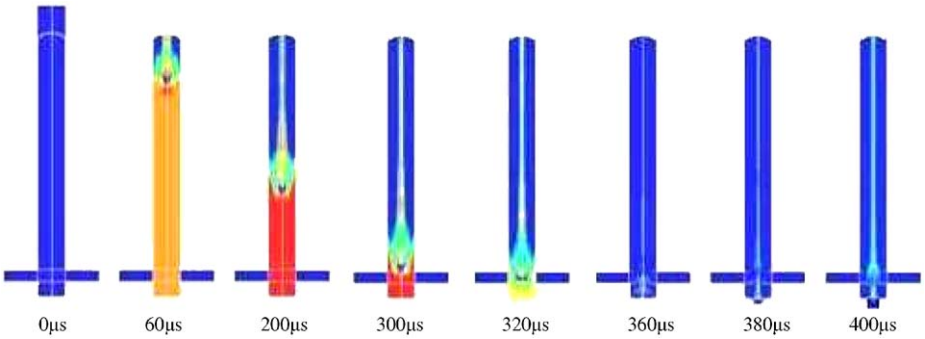

Fig. 10. The penetration process of EFP after 0.5 m flight.

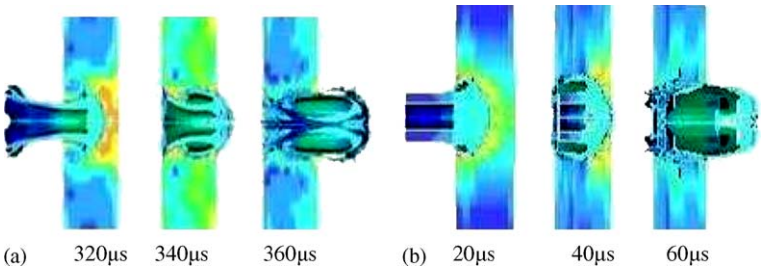

Fig. 11. The comparison of the penetration process between (a) EFP and (b) simulated EFP.

the projectile hits the steel target with a very high velocity. The material around the head produces plastic strain and a lot of heat is generated in this field. A strong shock wave is created in the steel target synchronously. Only a small pit occurred on the surface of the steel target because the head area of the projectile is small. Because of the high temperature and the friction the mass and the kinetic energy of the projectile decrease with the penetration. The area of the head increases due to the plastic strain and the penetration diameter increases.

In the second phase, the head penetrates the steel associate with the empennage. The acceleration is maximal when the empennage hits the steel target and the velocity decreases fast. Therefore, the penetration diameter in the steel target increases to the maximum. The diameter of the entrance increases because of the penetration effect of the empennage. The third phase is passing and flying out phase. Along with the increase of the penetration depth, the abrasion increases, the area of the projectile and the diameter of the hole decrease. When it flies out the steel target, the exit hole likes a lip. The projectile becomes fragments and flies out the steel target. The empennage of the simulated EFP does not enlarge the hole because it does not have the empennage.

4.2. The similarity of the velocity attenuation rules for the two kinds of projectiles

The velocity attenuation time history curves can be obtained from the above simulation result, which is shown in Fig. 12. From the figure, we can see that the attenuation rules are the same basically. The velocity of the projectiles decreases rapidly after they impact the steel target until they pass the steel target. Some differences exist in the curve because the simulated EFP has no empennage and the model is different from the real EFP.

The residual velocity of the projectile after it passed the steel target is an important index of the penetration ability of the projectile. It is a main method to simulate the penetration process using the simulated EFP instead of the real one because it is simple and economical. The result of the simulated EFP is different from the real situation because of the difference in the mass and structure. The residual velocity difference of the two projectiles affects the penetration ability, which will be studied below (Table 5).

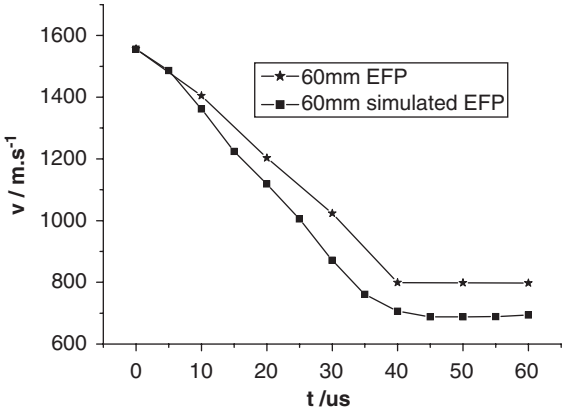

Fig. 12. The velocity attenuation time history curves of the simulated and the real EFP for the penetration process.

Table 5
The computed result for residual velocity of the real and simulated EFP

EFP	Before hit the target velocity V_1 (m/s)	Real EFP		Simulated EFP		Target thickness ξ (m)
		Mass M (kg)	Residual velocity V_2 (m/s)	Mass m (kg)	Residual velocity V_2 (m/s)	
60 mm	1556	0.0719	798	0.0672	694	0.025

The theory of the penetration process of EFP is similar to the penetration model of the bacilliform projectile. According to the friction movement mode, the resistant force comes from the shearing yield stress σ_{SY} when the fragment moves relatively to the other part. The sum of the resistant force equals to the product of the shearing yield stress σ_{SY} and the instantaneous contact area of fragment $2\pi R_p(h_t - x)$ with the other part. In the equation, x is the distance the projectile moved after impact. The expression of total friction resistant force is

$$F = 2\pi R_p(h_t - x)\sigma_{SY}. \tag{4}$$

The kinematic equation of the projectile and the fragment is

$$(m + \pi R_p^2 h_t \rho_t)\frac{dV}{dt} = -2\pi R_p(h_t - x)\sigma_{SY}. \tag{5}$$

By

$$\frac{dV}{dt} = V\frac{dV}{dx} = \frac{1}{2}\frac{d}{dx}V^2,\ \bar{V}_0 = \frac{m}{m + \pi R_p^2 h_t \rho_t}V_0,$$

Eq. (5) can be simplified as follows:

$$V_f^2 = \left(\frac{m}{m + \rho_t \pi R_p^2 h_t}\right)^2 (V_0^2 - V_{50}^2), \tag{6}$$

where V_f is the residual velocity of the projectile, V_0 is the initial velocity of the projectile, V_{50} is the limit penetration velocity of the projectile, m is the mass of the projectile, R_p is the radius of the projectile, ρ_t is the density of the steel target and h_t is the thickness of the steel target.

Table 6
The residual velocity of the real EFP obtained from the simulated EFP

EFP	V_0 (m/s)	Real EFP			Simulated EFP			Thickness ξ (m)	V_{f2} (m/s)	Relative error
		m_2 (kg)	V'_{f2} (m/s)	V'_{50} (m/s)	m_1 (kg)	V_{f1} (m/s)	V_{50} (m/s)			
60 mm	1556	0.0719	798	946	0.0672	694	915	0.025	725	9.1%

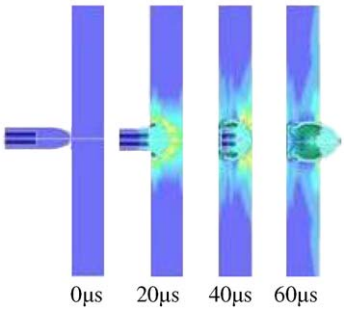

Fig. 13. The penetration process of the simulated EFP after 48 m flight.

The limit penetration velocity through the steel target of the projectile can be obtained by De Marre equation [11]:

$$V_c = k\,\frac{d^{0.75}h^{0.7}}{m^{0.5}\cos\alpha}.$$

The limit penetration velocity of the projectile V_{50} can take the value of V_c approximately.

By assuming that V_{f1} is the residual velocity of the simulated EFP and V_{f2} is the residual velocity of the real EFP, we can get Eq. (7) from Eq. (6).

$$V_{f2} = V_{f1}\left(\frac{m_2}{m_2+\rho_t\pi R_p^2 h_t}\right)\left(\frac{m_1+\rho_t\pi R_p^2 h_t}{m_1}\right)\sqrt{\frac{(V_0^2-V'^2_{50})}{(V_0^2-V_{50}^2)}}, \tag{7}$$

where V'_{50} is the limit penetration velocity of the real EFP, V_{50} is the limit penetration velocity of the simulated EFP, m_2 is the mass of the real EFP and m_1 is the mass of the simulated EFP.

If the residual velocity of the simulated EFP V_{f1} is known, the residual velocity of the real EFP can be obtained by Eq. (7). The computed result is shown in Table 6.

From Table 6, we can see that the residual velocity (V_{f2}) of the real EFP obtained from Eq. (7) is close to the result (V'_{f1}) from the whole process simulation of 60 mm EFP. The relative error is less than 10%.

4.3. The penetration process of EFP after 48 m flight

According to the above analysis, the penetration performance of the real EFP is studied through the simulated EFP. The projectile impacts the steel target after 48 m flight. The simulation result is shown in Fig. 13.

From the above simulation result, it is known that the simulated EFP can penetrate the steel target with the designed thickness. A part of the projectile is left in the steel target and a part flies out the steel target. The simulation result is coincident with the practical situation. The penetration effect at the entrance and the exit of the steel target is shown in Fig. 14. The color of figure indicates the contours of effective stress in steel target.

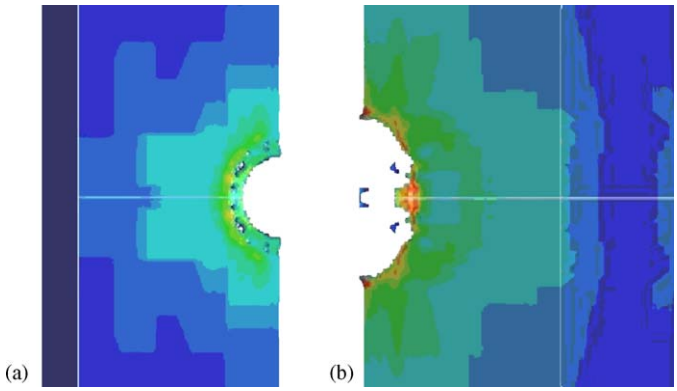

Fig. 14. The penetration effect at the (a) entrance and (b) exit.

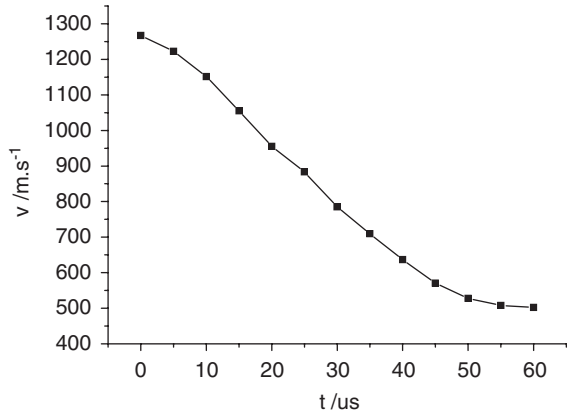

Fig. 15. The velocity attenuation curve in penetrating the steel target after 48 m flight.

Table 7
Simulation conclusion of the simulated EFP

EFP	V_1 (m/s)	ξ (m)	h (m)	m (kg)	V_2 (m/s)	d (mm)	Penetration status	D_{En} (mm)	D_{Ex} (mm)	D_{max} (mm)
60 mm	1267	0.025	48	0.0672	502	16.7	Penetrated	$\varphi 18 \times 18$	$\Phi 27 \times 24$	$\varphi 30$

Fig. 15 is the velocity attenuation curve of the simulated EFP in penetrating the steel target. The curve shows that the residual part of the projectile has a high velocity yet.

From the above analysis, we can get the property parameters of the simulated projectile, as shown in Table 7, where, V_1 is the velocity of the projectile when it hit the target, V_2 is the residual velocity of the projectile after it penetrated the target, D_{En} is the dimension of the entrance, D_{Ex} is the dimension of the exit and D_{max} is the maximum aperture.

5. Experimental study of the flight and penetration property

5.1. The charge structure and the experimental device

The length and the diameter of the charge is 66 and 60 mm, respectively. The weight of the dynamite is 198 g and 8701 dynamite is selected in the test. The diameter of the shaped charge cover is 56 mm and the shape of the cover combines arc and cone shapes. The charge cover and the charge structure are shown in Fig. 16.

The precession and nutation situation during the flight process are recorded by grid target. There are a series of targets on the way of the EFP flying. The holes of the projectile on the targets can reflect the change of the precession angle and nutation angle. Therefore, the flight stability of the projectile can be examined. There are eight grid targets with an interval of 2 m starting from 10 m to the projectile. The velocity and its reduction can be measured by two groups of aluminum foil. The steel target is 48 m far from the projectile, which is the distance of 800 times of the charge caliber. The grid targets device in the test are shown in Fig. 17.

5.2. *The flight stance test of EFP*

The shapes of holes are recorded using the grid target for three EFP in every group of the tests. Three EFP penetration pictures on the grid target are shown in Fig. 18. Generally speaking, the hole likes an egg if the nutation angle does not equal zero. The angle between the longitudinal axis and the vertical line is the precession angle r. The nutation angle can be determined according to the long and short axes if the dimension of the projectile is known. The dimension parameters can be optimized by the simulated EFP. Therefore, the history curve of the nutation angle can be obtained by the holes' shapes and the dimension of the EFP.

The initial disturbance to the flight of EFP occurs because of the unsymmetrical, the offset of the test device, and the real-time initiation for the projectile. The design of EFP can be used as reference of the formation mechanism and the shape of the collected projectile. The optimized EFP has a close-grained head and an enlarged empennage.

The shape of EFP must have an empennage like the missile to forbid the projectile from rotating. The stability of the projectile is good enough to meet the design demand. The moment formed by the shape is a kind of steady moment because of the gravity center at the fore part and the resistant force center at the back part of the projectile. The change of the incidence is a kind of harmonic vibration for the projectile with an empennage under the stable moment. The vibration of the projectile reduced very soon because of damping. Therefore, the whole system is a stable system.

The formation of EFP is good and does not break from the hole shaped on the grid target, which is shown in Fig. 18. The change property of incidence for the plane is from large to small and then to large. The change is periodical like a harmonic motion. Therefore, EFP swings periodically under the stable moment according

Fig. 16. The charge cover and the charge structure.

Fig. 17. The grid targets device in the test.

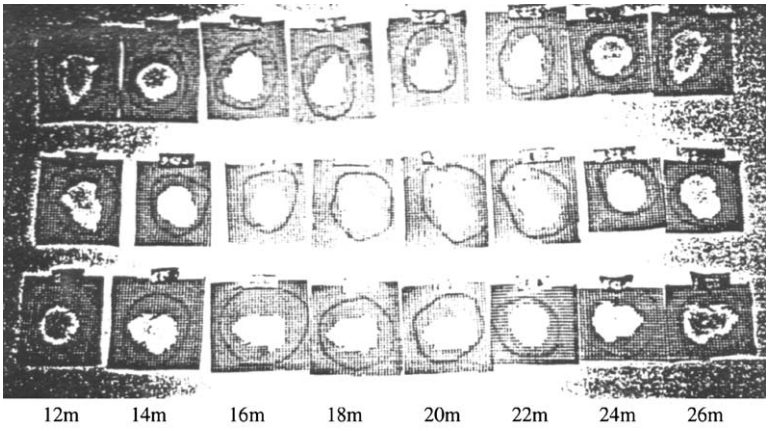

Fig. 18. The hole shapes recorded on the grid targets.

Table 8
The test velocity of EFP and its reduction

EFP	I target distance form detonation L_I (m)	Targets interval d_t (m)	I target velocity V_I (m/s)	II target velocity V_{II} (m/s)	Average velocity reduction R_v ($m\,s^{-1}$/m)
60 mm	10	33.5	1479	1256	6.01

to the test result. The flying of EFP is stable and the test velocity of EFP and its reduction are shown in Table 8.

5.3. Penetration property test of EFP

The penetration to a 25 mm thick steel target test is carried out for 60 mm EFP after flight distance of 48 m. The experimental result is shown in Table 9, the hole on the target and the falling pieces are shown in Fig. 19.

5.4. The comparison between the test and the simulation of EFP

The comparison between the test and the theoretical result of 60 mm EFP is shown in Table 10. The shape comparison between the simulation and the experimental projectile is shown in Fig. 20, where V_0 is the simulated initial velocity of EFP, V_I is the velocity after pass I target and V_{II} is the velocity after pass II target from the test data, $V_{f-0.5}$ is the velocity after 0.5 m flight predicted by Eq. (3), V_{48} is the predicted velocity of the projectile after 48 m flight. The other parameters have the same meaning as before.

The simulation and theoretical solution agree with the experimental data from the above results. The parameters for 60 mm EFP in the simulation and the parameters for the EFP in experiment are shown in Table 11.

The results of the simulation and experiment are consistent and the shape of the simulated projectile is as same as the real one. The simulation result is a little larger than that in the test in the velocity and the ratio of the length to the diameter. The mass of the projectile is a little larger than the simulated projectile.

6. Conclusions

(1) The results of numerical simulation and experiment analysis indicate that ideal shaped charge can be obtained if we adopt EFP charge structure and the shape of cover combining arc and cone. Such a charge

Table 9
Result of the penetration test of EFP

EFP	V_I (m/s)	Average velocity reduction R_v ($m\,s^{-1}$/m)	Steel target thickness ξ (mm)	Test result
60 mm	1479 (10 m far)	6.01	25	Penetrated at 48 m, Φ20–Φ30 mm(hole)

Fig. 19. The hole on the target and the falling pieces.

Table 10
The comparison between the test and the theoretical result

EFP	V_0 (m/s)	$V_{f-0.5}$ (m/s)	V_{48} (m/s)	V_I (m/s)	V_{II} (m/s)
60 mm	1563	1559.9	1267	1479 (10m)	1256(43.5 m)

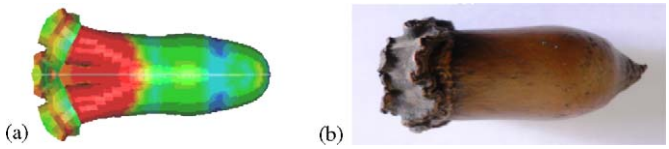

Fig. 20. The shape comparison between the simulation and the experimental projectile: (a) The shape of 60 mm simulated EFP and (b) the shape of 60 mm experimental EFP.

Table 11
The simulation parameters for 60 mm EFP and the parameters for the experimental EFP

EFP	Velocity (m/s)	Length (mm)	Diameter (mm)	Length/diameter	Mass (g)
Simulation	1563	47.6	16.7	2.85	71.9
Experiment	1479	40.0	15.0	2.67	74.1

is of high-flying velocity and ideal ratio of the length and the diameter. In addition, it is of good flutter and penetration property.

(2) It is impractical and difficult to simulate the whole process including a long flight distance for studying velocity attenuation law of EFP. This paper adopts ALE method to simulate a flight distance of 0.5 m. The results forecast by EFP velocity attenuation theory coincide with numerical simulation, which indicate that the forecasting is reasonable and the simulation method is accurate. Based on this theory, the velocity after EFP flies a longer distance can be forecast by this attenuation law, as the following: the velocity of

completely formed 60 mm EFP is 1563 m/s, while it reduces to 1267 m/s after a flying distance of 48 m. The average velocity decrease with distance is approximate to 6.4 m/s/m, which is consistent with the experimental results (velocity decreases with distance is 6.01 m/s/m).

(3) According to the similarity theory, the method of simulating the penetration process of EFP instead of simulated EFP can overcome the technical difficulty of simulating the whole process of long distance and penetration. But the different quality of simulated EFP and real one may lead to different results to some extent. After 0.5 m flight and penetrating the target, the residual velocity of EFP investigated by simulated EFP can be compared with the numerical simulation. The comparison shows that the error is less than 10%. Furthermore, it indicates that the residual velocity after penetration can be obtained approximately from simulation. At the same time, it is practical to study the penetration property of EFP by using simulated EFP which is similar to the real one in shape and quality.

(4) The 60 mm EFP and the simulated EFP with the velocity after flying 48 m strike the 45 #steel target of 25 mm thick. The results of numerical simulation and experiment both show that they can fly through the steel target, resulting in its broken chips burst away at a fast velocity.

(5) The flight stability and the penetration ability are studied by experiment in this paper. The simulation and theoretical results can meet the experiment. This shows that the simulation can reasonably predict the formation shape, mass, velocity, flight stability, penetration ability of the projectile. The ALE technique can achieve the work to simulate the fluid–solid coupling problem well. The methodology developed in this paper can be used by engineers to design EFP.

Acknowledgements

The work presented in this paper has been funded by the National Natural Science Foundation of China under No. 50578082.

References

[1] Pappu S, Murr LE. Hydrocode and microstructural analysis of explosively formed penetrators. J Mater Sci 2002;37(2):233–48.
[2] Ng W, Fong R, Rice B. Hydrocode 3D simulation of non-axisymmetric explosively-formed projectile (EFP) warheads. In: Proceedings of 17th International Symposium on Ballistics, Midrand, South Africa, 1998. p. 481–7.
[3] Wang C, Yun SR, Huang FL. Numerical simulation on jet formation by wide angle shaped charge and penetration into multilayer targets. Explo Shock Wave 2003;23(4):349–54.
[4] Yu C, Tong YJ, Yan CL, et al. Applied research of shaped charge technology. Int J Impact Eng 1999;23(1 (part 2)):981–8.
[5] Weimann K. Flight stability of EFP with star shaped tail. In: Proceedings of 14th International Symposium on Ballistics, Quebec, Canada, 1993. p. 755–63.
[6] Johnson GR, Stryk RA. Some considerations for 3D EFP computations. Int J Impact Eng 2006;32(10):1621–34.
[7] Yu C, Dong QD, Sun CW. The experimental studies of explosively formed projectile with star shaped tail. Explo Shock Wave 2003;23(6):561–4.
[8] Carleone J, Bender D. A unique method of providing an explosively formed projectile with fins. In: Proceedings of 17th International Symposium on Ballistics, Midrand, South Africa, 1998. p. 55–62.
[9] Hallquist JO, LS-DYNA User's Manual. LSTC, 1997. p. 34–109.
[10] Johnson GR, Cook WH. A constitutive model and data for metals subjected to large strains, high strain rates and high temperatures. In: Proceedings of Seventh International Symposium on Ballistics, Hague, Netherlands, 1983. p. 541–7.
[11] Wang Lili, Yu Tongxi, Li Yongchi. Progress of impact dynamics. University of Science and Technology of China Press; 1992. p. 56–90.